ACS APPLIED POLYMER MATERIALS

pubs.acs.org/acsapm Article

Fully Deformable Dual-Stopband Photonic Microcapsules via Microfluidic Core−Shell Emulsion Templates: Tunable Optical Properties and Mechanical Responsiveness

Yu Bai, Yi Ding, Guoquan Liao, Xiangchun Kong, Yucheng Wang, Mingshuo Dai, and Yuandu Hu*

Cite This: ACS Appl. Polym. Mater. 2026, 8, 3658−3667 Read Online

ACCESS | Metrics & More | Article Recommendations | Supporting Information

ABSTRACT: Photonic microcapsules with dual stopbands hold great potential in sensing and wearable electronics. However, existing systems face limited deformability and responsiveness to physical stimuli. In this study, we fabricated fully deformable dual-stopband photonic microcapsules using microfluidics-enabled core−shell double-emulsion templates. The core and shell parts of the microcapsules were an aqueous suspension of PNIPAM-*co*-AAC hydrogel particles and a poly(ethylene glycol) phenyl ether acrylate (PEGPEA) resin suspension of silica particles, respectively. Given that the core and shell parts were both deformable components, the resultant photonic microcapsules featured full deformability. Their structural colors can be regulated by tuning the particles' diameters and volume fractions. The resultant microcapsules exhibited isotropic reflection spectra, overcoming angle dependence, and showed reversible color changes under mechanical compression. This work offers a scalable approach for multifunctional photonic microcapsules, paving the way for applications in microsensors, stress visualization, and adaptive wearable devices.

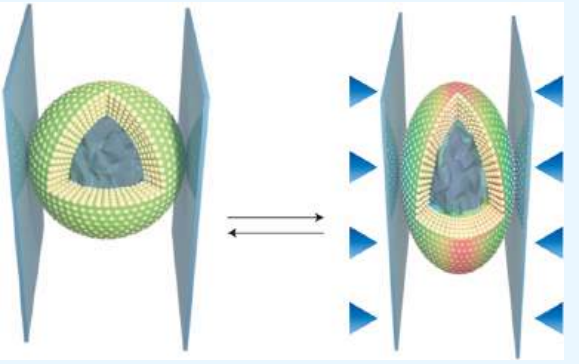

KEYWORDS: *microfluidics, photonic microcapsules, dual stopbands, full deformability, mechanical response*

INTRODUCTION

Photonic microparticles are widely used in many industries, such as sensors, displays, coding and decoding, and pigments.[1−7] Microfluidics is a potent platform that can precisely and carefully mold and adjust the characteristics of photonic microparticles.[8−11] Creating photonic microparticles with various geometries and characteristics has attracted much research interest throughout the last two decades.[12−17] Simple photonic characteristics, like a single stopband, are present in most of the resultant photonic microparticles.[18−20] The constant development of technology demands researchers to develop photonic micro-objects capable of combining more functions, namely multifunctionalities. One aspect of multifunctionalization is featuring photonic microparticles with more than one stopband.[21] Researchers have built a variety of photonic micro-objects with dual stopbands and beyond in this context.[22,23] To fabricate photonic micro-objects with multiple stopbands, photonic micro-objects can integrate several photonic compositions in a core−shell, Janus, or multicompartmental fashion. For instance, Janus/multicompartment photonic microparticles with dual stopbands and beyond were created by Chen, Gu, and Kim et al., respectively.[21,24−31] Janus-type photonic microparticles' angle-dependent optical characteristics could be problematic in some situations. This has enabled the development of photonic microparticles with core−shell or quasi-core−shell architectures, in which each of the core and shell portions usually exhibits unique optical properties.[32−34] Using the color mixing technique, Kim et al. recently developed triple stopband photonic microcapsules in which the core contains all the photonic compositions. However, it is impossible to manipulate the color pixels in a precise manner within the individual microcapsule.[35] Furthermore, most photonic microcapsules are stress-resistant, which can be a drawback for applications in wearable electronics that use them to sense mechanical stimuli such as stress.[36] Despite the development of mechano-deformable hydrogel photonic microcapsules with dual stopbands by Gu and Li et al., respectively, the all-hydrogel matrix might only be applicable in specific environments, such as water solutions.[37,38] Therefore, we demonstrate the creation of photonic microcapsules with dual stopbands and fully deformable characteristics with the assistance of microfluidics. By using an aqueous suspension of poly(*N*-isopropylacrylamide-*co*-acrylic acid) (PNIPAM-*co*-AAC) gel particles as the core and a photocurable poly(ethylene glycol) phenyl ether acrylate

Received: December 15, 2025
Revised: February 20, 2026
Accepted: February 24, 2026
Published: March 2, 2026

https://doi.org/10.1021/acsapm.5c04701
ACS Appl. Polym. Mater. 2026, 8, 3658−3667

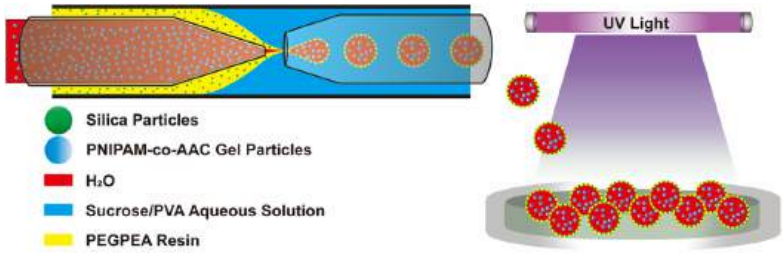

Figure 1. Schematic diagram of the preparation of fully deformable dual-stopband photonic microcapsules assisted by the microfluidic technique.

(PEGPEA) resin dispersion of SiO_2 particles as the shell, core−shell droplets were successfully fabricated via microfluidics. Upon ultraviolet (UV) exposure for photocuring, the core−shell droplets were polymerized into photonic microcapsules. Owing to the optical properties of the initial core and shell phases, the photonic microcapsules exhibited dual stopbands, with each structural layer contributing to a distinct stopband. Furthermore, the generated photonic microcapsules are fully deformable due to the softness of the gel particles and the elastic properties of the PEGPEA resin.[18,39] In particular, when subjected to mechanical compression, the photonic microcapsules showed dramatic color changes because of the changes in the internal photonic structure. These microcapsules could be building blocks for wearable electronics and microsensors.

EXPERIMENTAL SECTION

Materials

Poly(vinyl alcohol) (PVA, M_w = 13,000 g/mol−23,000 g/mol), poly(ethylene glycol) phenyl ether acrylate (PEGPEA, $M_w \sim 324$ g/mol), ethoxylated trimethylolpropane triacrylate (ETPTA, $M_w \sim 428$ g/mol), and sodium dodecyl sulfate (SDS) were purchased from Sigma-Aldrich. Tetraethyl orthosilicate (TEOS), ammonia solution (≥28% NH_3 in water), *N*-isopropylacrylamide (NIPAM), acrylic acid (AAC), *N*,*N*′-methylenebis(acrylamide) (BIS), sucrose, potassium persulfate (KPS), and triethoxy-1H,1H,2H,2H-tridecafluoro-n-octylsilane were purchased from Aladdin. Ethanol was purchased from Beijing Chemical Reagent Co., Ltd. 3,3-Dimethoxy-2,7,10-trioxa-3-silaundecane was purchased from Bidepharm. The photoinitiator 2-hydroxy-2-methylpropiophenone (1173) was purchased from TCI. All chemicals were used as received. Deionized (DI) water was produced from a Milli-Q Direct system (Merck, Shanghai, China).

Preparation of PNIPAM-*co*-AAC Gel Suspensions with Different Structural Colors

1.06 g of NIPAM, 0.06 g of BIS, 0.018 g of SDS, and 0.09 g of AAC were mixed with 70 mL of DI water. The mixture was stirred until it was completely dissolved. Subsequently, the solution was transferred to a 250 mL three-neck flask. Separately, 0.03 g of KPS was dissolved in 10 mL of DI water. The solution in the three-neck flask was placed under nitrogen protection (50 mL/min nitrogen flow), heated to 80 °C, and stirred at 250 rpm. Upon reaching 80 °C, the KPS solution was slowly added to the flask. As polymerization began, white turbidity appeared in the solution, indicating the onset of the reaction. After 4 h, the reaction was deemed complete, and the flask was promptly removed and placed into ice water to cool down to room temperature, halting the reaction. The resulting product was well-dispersed PNIPAM-*co*-AAC gel particles (the structural formula is shown in Figure S1a). These gel particles' sizes can be adjusted by changing the amount of KPS.

After synthesizing the gel particles, the solution was placed in a convection oven set to 55 °C for 12 h, enabling us to evaporate a certain amount of water, and then cooled to room temperature. Based on the above findings, gel particles were successfully synthesized. After undergoing evaporation and subsequent cooling processes, these gel suspensions exhibited blue, green, and red structural colors.

Preparation of Photocurable Resins Dispersions of Silica Particles

In a 250 mL conical flask, 22 mL of ethanol and 5 mL of ammonia solution were mixed and thermostated in a water bath at 50 °C for 10 min. Under continuous stirring at 350 rpm, a premixed solution containing 22 mL of ethanol and 0.8 mL of TEOS was added dropwise. After 30 min, 4 mL of an ammonia solution was supplemented to the reaction mixture. Following an additional 10 min of stirring, a second mixture composed of 44 mL of ethanol and 1 mL of TEOS was introduced, and the reaction mixture was allowed to proceed for 6 h to complete the synthesis. Upon completion of the synthesis, the resulting silica dispersion was washed with ethanol and subjected to centrifugation to remove the supernatant, which was repeated three to four times. The collected precipitate was subsequently dried in an oven at 70 °C to obtain a silica particle powder. The silica particles were then redispersed in ethanol and treated with ultrasonication for 1 h to ensure thorough dispersion. The size of the silica particles could be effectively controlled by adjusting the temperature.

A PEGPEA resin (the structural formula is shown in Figure S1b) containing 1 w/w% of photoinitiator 1173 was added to the ethanol dispersion of SiO_2 particles. The volume fraction of silica can be regulated by the amount of silica ethanol dispersion added. Typically, we use a resin suspension with silica at a 25% volume fraction. Following 30 min of additional ultrasonication, the mixture was placed in a convection oven at 70 °C and dried for 12 h to evaporate the ethanol selectively. This process yielded a light-curable resin with a structural color. Preparation of the ETPTA resin suspension followed the same procedure as the PEGPEA one.

Construction of Microfluidic Devices

The glass capillary microfluidic device used in our experiments consisted of two coaxially aligned cylindrical capillary tubes with tapered tips within a square capillary tube. The round capillary had an inner diameter of 0.58 mm and an outer diameter of 1 mm. In comparison, the square capillary had an inner diameter of 1.05 mm and an outer diameter of 1.1 mm. Two round capillaries were thermally fused at their termini and precision-polished to generate distinct tip configurations for specialized experimental applications. The injection tube with a relatively smaller tip (110 μm) was treated with triethoxy-1H,1H,2H,2H-tridecafluoro-n-octylsilane to make it hydrophobic. The collection tube (tip diameter: 380 μm) was treated with 3,3-dimethoxy-2,7,10-trioxa-3-silaundecane to impart hydrophilicity. The two capillaries were then aligned with 100 μm spacing. Needles were attached and fixed to the device by using epoxy structural adhesive to ensure stability and operational precision.

Preparation of Fully Flexible Dual-Stopband Photonic Microcapsules

Water-in-oil-in-water (W/O/W) double-emulsion droplets with dual stopbands were created using a microfluidic technique. As shown in Figure 1, three syringe pumps (NE-1000) were used to inject the three different phases: an inner gel suspension phase (with gel particles of average diameters 187, 236, and 276 nm corresponding to blue, green, and red structural colors, respectively), a resin-based intermediate phase (PEGPEA resin containing silica particles at a volume fraction of 25 vol %), and an outer sucrose/PVA aqueous phase (16 wt % sucrose and 1.8 wt % PVA) through separate inlets. Monodisperse core−shell

https://doi.org/10.1021/acsapm.5c04701
ACS Appl. Polym. Mater. 2026, 8, 3658−3667

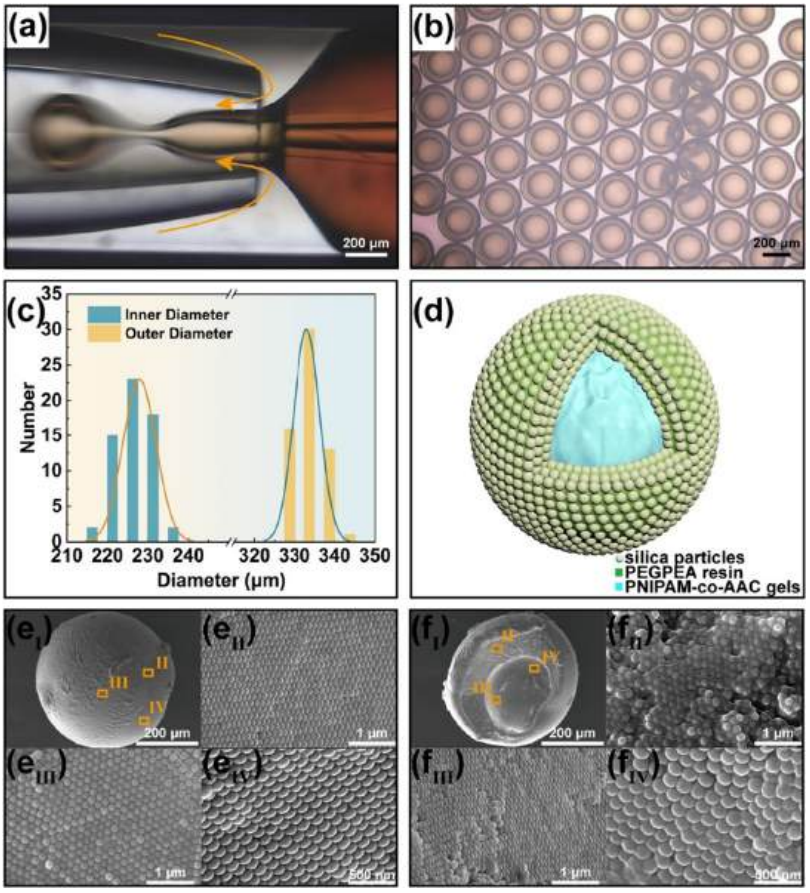

Figure 2. (a) Microscopic photographs documenting the process of preparing double-emulsion droplets via a microfluidic device. (b) Microscopic pictures of the prepared double-emulsion droplets. (c) Statistical distribution of double-emulsion droplets' outer shell and inner core sizes. (d) Schematic diagram of the microcapsule. (e) SEM image of the microcapsule surface. (f) SEM image of the microcapsule cross-section.

droplets were successfully generated by independently controlling the flow rates of each phase (e.g., 30 μL of h^{-1} for the inner phase, 100 μL of h^{-1} for the intermediate phase, and 2000 μL of h^{-1} for the outer phase), and the droplets were collected into a sucrose/PVA aqueous solution and photocured when exposed to 365 nm UV light for 30 s. Adjusting the flow rates of each phase allowed precise control over parameters such as the shell thickness and core size of the double-emulsion droplets (Figure S2).

Characterizations

The microcapsule preparation process was observed and photographed by using an optical microscope in transmission mode (Shanghai Cewei Optoelectronics Co., Ltd., China). The microcapsules' structural colors were observed using an optical microscope in reflection mode (Olympus BX53M), and the reflectance spectra were recorded using a fiber-optic spectrometer (Ocean Insight, Inc.). After 2 weeks of dilution and dialysis, the gel particles were freeze-dried, and the morphologies and dimensions were observed under a scanning electron microscope (SEM) (CLARA, Tyscan). The diameter and distribution of the gel particles were analyzed by using DLS equipment (Malvern Panalytical). The refractive index of the gel was determined by using an Abbe refractometer (Biam BM-2WAJ). An SEM (Hitachi UHR FE-SEM SU8000) was used to characterize the surface of the microcapsules and the arrays of silica particles in the cross-section. A transmission electron microscope (TEM) (JEOL JEM-1400) was used to observe the size and uniformity of the silica particles. The mechanical strength of the microcapsules was characterized by using a particle strength tester (SKZ-500, Xiangyi Instrument, China). The osmotic pressure was measured by using a freezing point osmometer (Advanced Instrument). Mechanical properties of PEGPEA resin (with 25 vol % silica) were tested using a universal material testing machine (Instron 5942, Instron). Rheological measurements of the PNIPAM-*co*-AAC gel were conducted with a rheometer (Haake Mars 40, Haake, Germany).

RESULTS AND DISCUSSION

The reliable production of monodisperse droplets using the microfluidic technique marked the beginning of the fabrication process, which is depicted in Figure 2a and shown in Video S1. The microscope images of the photocured microcapsules are shown in Figure 2b. The accuracy of microfluidic processing was highlighted by the remarkable size homogeneity (CV < 3%) shown by statistical analysis of core and shell dimensions (Figure 2c). The schematic diagram of the microcapsule mechanism is shown in Figure 2d. The shell part was made of PEGPEA resin packed with silica particles. Specifically, silica particles (volume fraction exceeding previously reported crystallization threshold) were dispersed in the PEGPEA resin containing 1 wt % 1173 photoinitiator. Particle silanol groups and resin acrylate moieties formed hydrogen bonds, which improved interparticle repulsion and allowed the particles to self-assemble into non-close-packed face-centered cubic (fcc) lattices. The ordered silica particle arrangement and well-defined core−shell architecture were validated by SEM characterizations of the surface and cross-sectional morphologies (Figure 2e,f).

The structural color of the photonic resin was found to originate from the non-close-packed fcc arrangement of the silica particles. By carefully adjusting the sizes and volume fractions of silica particles, the structural colors of the photonic

https://doi.org/10.1021/acsapm.5c04701
ACS Appl. Polym. Mater. 2026, 8, 3658−3667

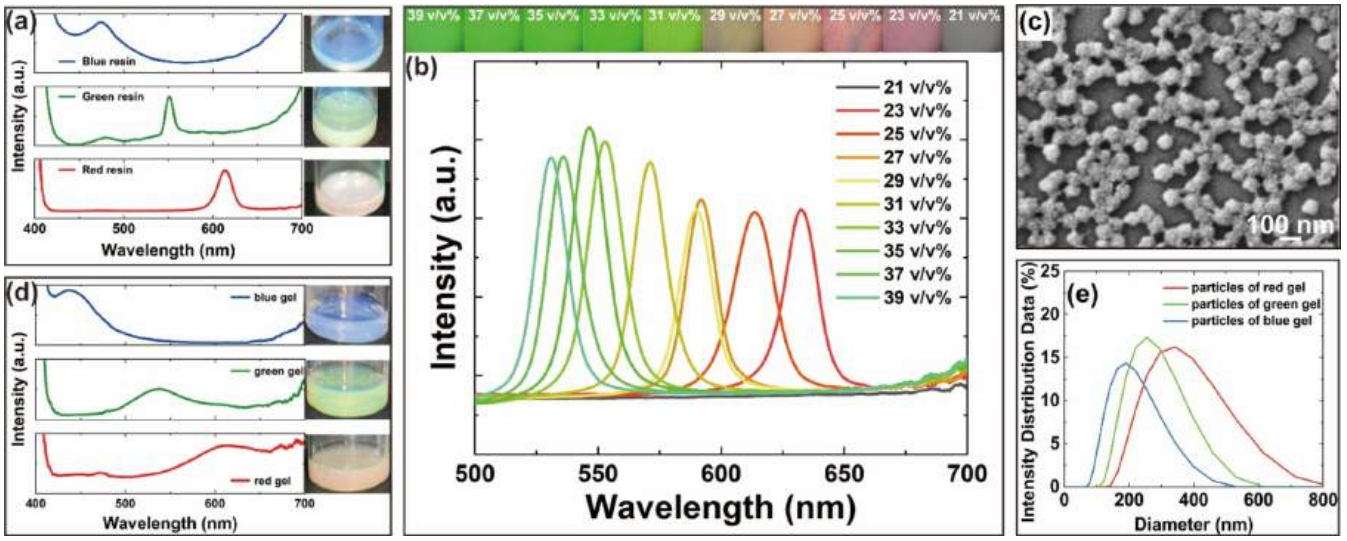

Figure 3. (a) Reflectance spectra and photographs of photonic PEGPEA resins with blue, green, and red colors prepared by silica particles with different diameters at a volume fraction of 25 vol %. (b) Photographs of the resin suspensions prepared by dispersing silica with the same average diameter in PEGPEA resin at different volume fractions and the corresponding reflectance spectra. (c) SEM images of PNIPAM-*co*-AAC gel particles after freeze-drying. (d) Reflectance spectra and photographs of photonic PNIPAM-*co*-AAC gel dispersion with blue, green, and red colors prepared by gel particles with different diameters. (e) Diameter distribution curves of gel particles corresponding to three-colored gel suspensions measured by DLS.

resin suspension demonstrated dynamic tunability. Based on Bragg's equation that has been modified

$$\lambda = 2dn_{\text{eff}} = \left(\frac{\pi}{3\sqrt{2}\varphi}\right)^{1/3}\left(\frac{8}{3}\right)^{1/2} D \left(n_{\text{silica}}^2\varphi + n_{\text{PEGPEA}}^2(1-\varphi)\right)^{1/2} \quad (1)$$

where d is the lattice plane spacing, n_{eff} is the effective refractive index (RI), which can be estimated from the Maxwell-Garnett average of the RI of the silica particle, n_{silica} = 1.45, and the RI of the PEGPEA matrix, n_{PEGPEA} = 1.502.[40] And φ is the volume fraction of the particle. D is the diameter of the particle.

When the volume fraction φ = 0.25, resins fabricated with silica particles exhibit reflection wavelengths of 474, 556, and 615 nm (corresponding to blue, green, and red hues, respectively), as shown in Figure 3a. These silica particles have TEM-measured average diameters of 135, 163, and 178 nm (Figure S3a–c), with size distribution statistics presented in Figure S3d–f. Based on these TEM-derived average particle sizes, the theoretical reflection wavelengths were calculated via eq 1 as 471, 569, and 622 nm, respectively, showing good agreement with the experimental results.

As shown in Figures 3b and S4, silica with an average diameter of 178 nm was dispersed in PEGPEA resin at different volume fractions from 21% to 39% to prepare photonic resin dispersion. No structural color was observed when the volume fraction of silica particles in the resin was 21 vol %, below the crystallization threshold, suggesting the absence of an ordered photonic structure. The resin exhibited a clear red hue with a reflection peak value at 632 nm, exhibiting a mere 1.1% deviation from the theoretical value of 639 nm, as the volume fraction rose to 23 vol %. With the volume fraction increased steadily, the particle spacing became smaller, and the hue of the resin suspension underwent a gradual blue shift. When the volume fraction increased to 39 vol %, the reflection spectrum peak was at 530 nm, which showed a deviation of 0.6% from the calculated value of 533 nm. The intensity of the reflection peaks increased as the volume fraction increased, suggesting that the silica particles were more closely and orderly arranged in the resin matrix.

The structurally colored aqueous suspension of PNIPAM-*co*-AAC hydrogel particles, which self-assembles into periodic aqueous arrays to achieve photonic stopband effects, was synthesized as detailed in the Experimental Section. As shown in Figures 3c and S5, SEM images of the freeze-dried gel particles (with water preserved) and statistical size distribution analysis indicate good size uniformity, and the average diameter of the freeze-dried gel particles in Figure 3c is 80 nm. Similar to the color regulation mechanism of the resin suspension, the structural color of the aqueous suspension of gel particles can be tuned by altering the volume percentage or particle diameter of the gel particles. Three-colored hydrogels were prepared by precisely adjusting the diameters of the fabricated gel particles (Figure 3d). We performed DLS measurements on the gel particles (with water contained) corresponding to the three-colored gel suspensions, and the results are shown in Figure 3e. The diameter distribution curves reveal that the particle diameters in the blue, green, and red gel suspensions increase sequentially, with average diameters of 187, 237, and 276 nm.

For the PNIPAM-*co*-AAC gel-particle-based colloidal crystal system, measuring the volume fraction of gel particles is difficult. Instead, we determined the system's effective refractive index ($n_{\text{PNIPAM-co-AAC}}$ = 1.3551) via an Abbe refractometer. Substituting $n_{\text{PNIPAM-co-AAC}}$ and the reflection peaks of blue (436 nm), green (537 nm), and red (612 nm) gels (Figure 3d) into eq 1, we calculated the (111) interplanar spacings as d_1 = 161 nm, d_2 = 200 nm, and d_3 = 226 nm.

Assuming gel particles are spherical and assemble in an fcc close-packed lattice, we used the fcc (111) spacing–particle diameter relationship (eq 2)

$$D = \sqrt{\frac{3}{2}} \cdot d \quad (2)$$

The results are D_1 = 197 nm, D_2 = 245, and D_3 = 277 nm. The observation that the theoretical diameters are slightly larger than

https://doi.org/10.1021/acsapm.5c04701
ACS Appl. Polym. Mater. 2026, 8, 3658–3667

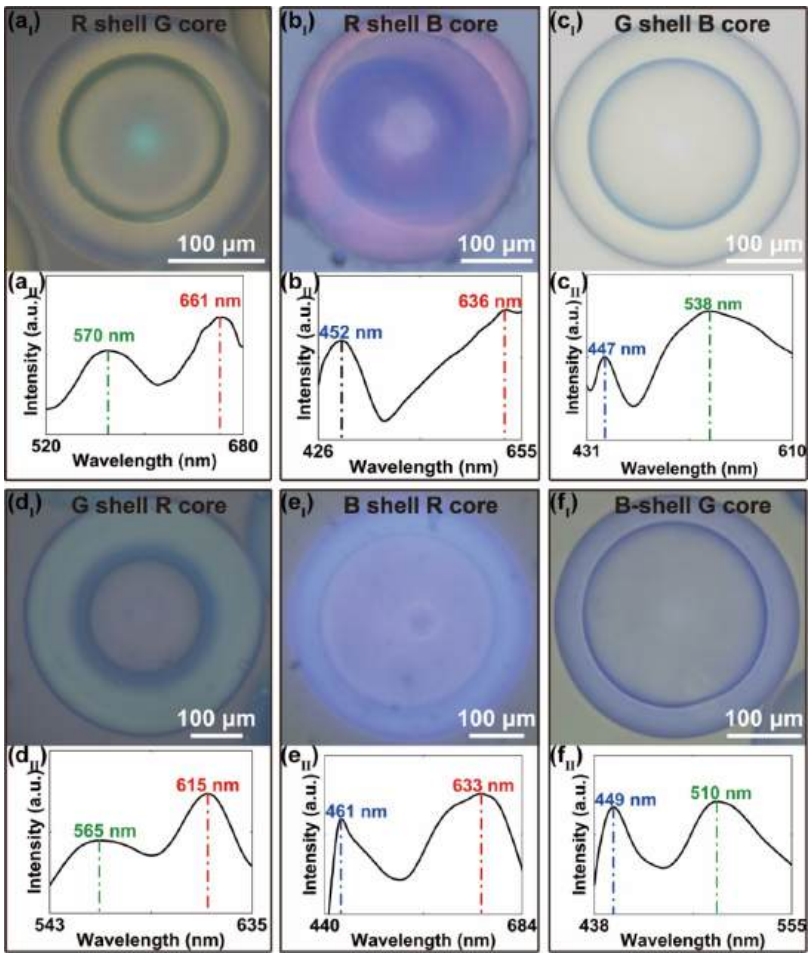

Figure 4. Six different dual-stopband microcapsules were fabricated by using distinct combinations of core and shell suspensions. The microscope images of six distinct combinations and their corresponding reflection spectra are as follows: (a) Red shell−green core; (b) red shell−blue core; (c) green shell−blue core; (d) green shell−red core; (e) blue shell−red core; (f) blue shell−green core.

the DLS measured values (187, 237, and 276 nm) suggests that tiny gaps exist between particles during actual assembly, which provides important insights for understanding the assembly behavior of gel-based photonic crystals.

These results led to the preparation of red, green, and blue PEGPEA resin suspensions and red, green, and blue PNIPAM-*co*-AAC gel particle suspensions as shell and core materials to create microcapsules with six combinations of structural colors. Their morphologies and structural colors were observed under an optical microscope, and the reflection spectra were measured using an optical fiber spectrometer, as shown in Figure 4a−f. It can be seen that the core and shell have distinct structural colors, which were further verified by the microcapsules' reflection spectra. The peaks at two different positions were used to confirm the presence of dual stopbands. The wide peaks in the inner core and shell layers suggested that the silica or hydrogel particles were likely in a photonic glassy state and had a short-range ordered arrangement, giving the microcapsules isotropic optical characteristics. This isotropic characteristic avoided errors brought about by varying viewing directions. Figure S6 presents photographs of the microcapsules, intuitively demonstrating their practical direct visualization effect. Furthermore, we created double-emulsion droplets with an average shell thickness of 6.6 μm. As shown in Figure S7, the entire microcapsule displayed the green color of the interior gel, since the shell layer was too thin to exhibit its structural color.

The PNIPAM-*co*-AAC gel encapsulated in the microcapsule core exhibits distinct temperature-responsive structural color behavior, which is closely associated with the thermosensitive phase transition of the PNIPAM-based materials. As illustrated in Figure S8a, when the microcapsules (with pure PEGPEA shells) are heated from 27 °C, the green color of the core part gradually fades to white, and this color change is fully reversible upon cooling to the initial temperature. Corresponding reflectance spectra (Figure S8b,c) further confirm this responsiveness. The characteristic reflectance peak of the gel core decreases progressively in intensity with increasing temperature, eventually disappearing accompanied by a slight blue shift, while the peak reappears and nearly restores to its original position (with a minor reduction in intensity) when the temperature returns to 27 °C. The slight attenuation in peak intensity after temperature cycling is attributed to the mild disruption of the ordered arrangement of gel particles during the phase transition and recovery process. For the dual-photonic stopband microcapsules, the green core transforms into diffuse blue and subsequently becomes colorless with an increase in temperature, and the original color is retrieved as the temperature decreases (Figure S9). This reversible temperature-responsive structural color change originates from the thermosensitive phase transition (lower critical solution temperature, LCST) of the PNIPAM-*co*-AAC gel: below the LCST, the gel particles exhibit hydrophilicity, leading to swelling

https://doi.org/10.1021/acsapm.5c04701
ACS Appl. Polym. Mater. 2026, 8, 3658−3667

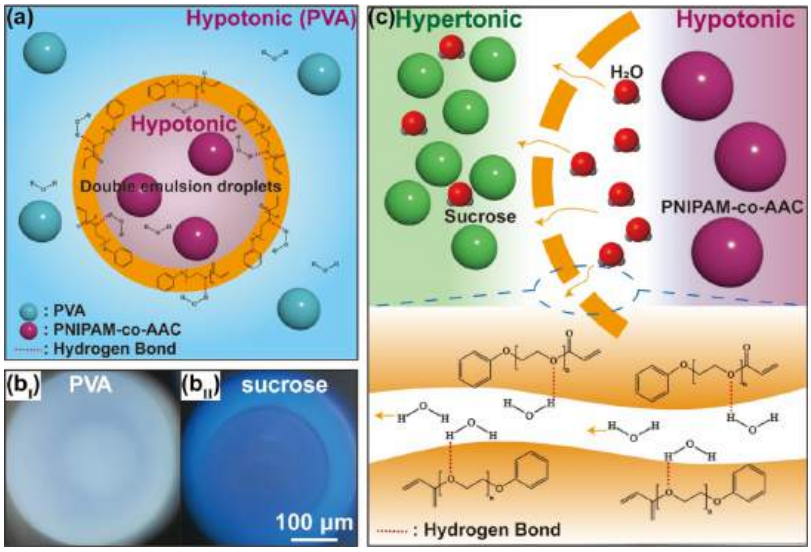

Figure 5. (a) Schematic diagram of hydrogen bond formation in hypotonic PVA external phase. (b_I) Microscopy images of microspheres with an aqueous solution of 10 wt % PVA as the external phase. (b_{II}) Microscopy images of microspheres with the external phase containing 16 wt % sucrose and 1.8 wt % PVA. (c) Schematic illustration of hypertonic sucrose external phase improving the optical quality of double emulsions.

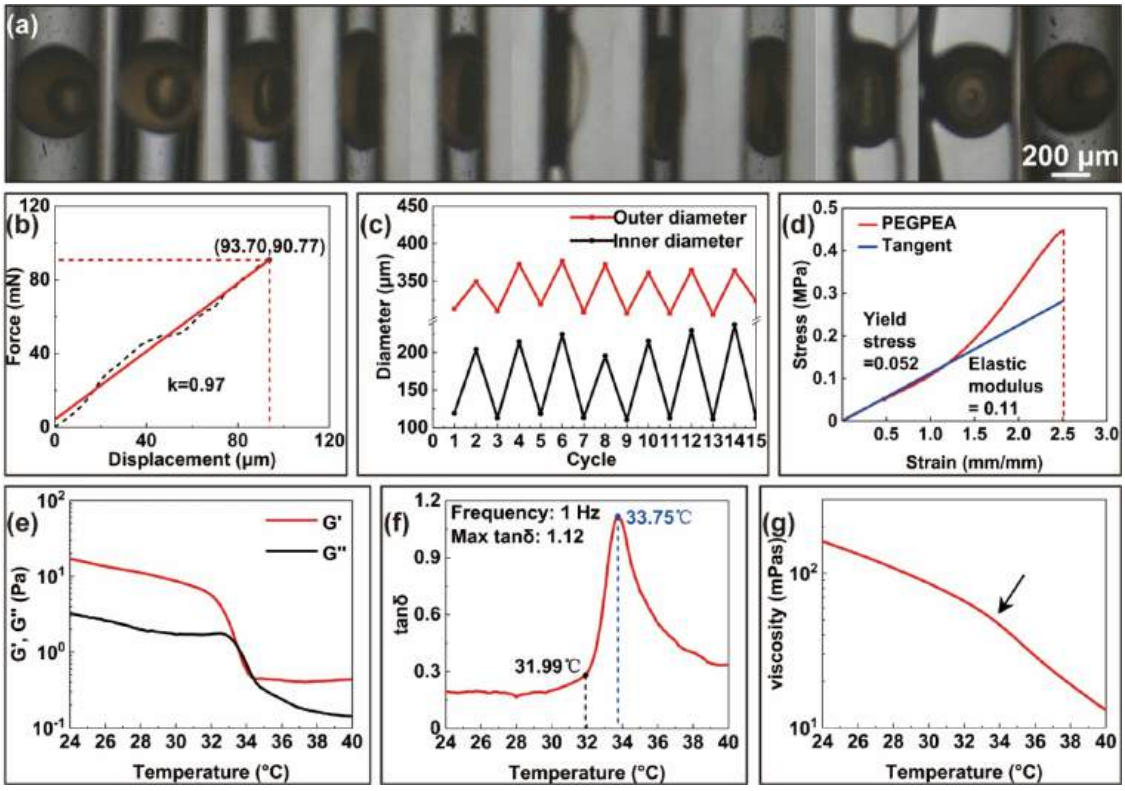

Figure 6. (a) Microscope photos of the process in which the microcapsules deform when squeezed and return to their original shape after the squeezing is removed. (b) Force−displacement curves corresponding to the process of microcapsule deformation until crushing. (c) Change curves of the inner and outer diameters of the microcapsules during the 15 compression−release cycles. (d) Stress−strain tensile curves for PEGPEA with 25 vol % silica. (e) Storage modulus (G′) and loss modulus (G″) of the PNIPAM-*co*-AAC gel as a function of temperature. (f) Loss factor (tanδ) of the PNIPAM-*co*-AAC gel as a function of temperature. (g) Viscosity of the PNIPAM-*co*-AAC gel as a function of temperature.

and maintaining an ordered arrangement that supports the characteristic structural color; as the temperature exceeds the LCST, the gel undergoes a "hydrophilic to hydrophobic" transition, triggering the collapse and shrinkage of gel particles. This phase-induced morphological change disrupts the ordered periodic structure of the gel, altering the photonic bandgap and thus causing the fading or shift of the structural color. Upon cooling back below the LCST, the gel particles revert to a hydrophilic state, reswell, and reestablish their ordered arrangement, resulting in the recovery of the original structural color.

Despite the fabrication of photonic microcapsules with dual stopbands, the structural colors in the microcapsules were not as vivid as those in bulk resin suspensions. We explored the underlying mechanisms contributing to this discrepancy. It has

https://doi.org/10.1021/acsapm.5c04701
ACS Appl. Polym. Mater. 2026, 8, 3658−3667

been reported that water molecules have a small solubility in PEGPEA, which reduces its optical quality.[41] The strategy of osmotic pressure-mediated regulation of the structural colors of photonic microcapsules has been reported.[42] High-osmotic-pressure sucrose solution suppressed water penetration into PEGPEA during single-emulsion microsphere preparation, which improved the optical quality.[43] The schematic diagram of this scheme is shown in Figure S10a. Based on the above-mentioned method, monodisperse single-emulsion droplets' microscope images and reflection spectra are shown in Figure S10b−d. It was observed that the microspheres' reflection peaks showed broader peak widths and significantly lower intensities than the bulk resin suspensions. This is because when silica particles assemble within droplets, they are affected by factors such as fluid shear force and surface tension and are prone to forming local defects or short-range ordered structures, which in turn leads to broadening of the reflection spectrum and a decrease in color performance.

In the core−shell double-emulsion system, we analyzed the effects of external phase osmotic pressure on the optical quality of photonic microcapsules. As shown in Figure 5a, PEG segments of the PEGPEA shell interact with both external and core water. When the external phase was a 10 wt % PVA aqueous solution with relatively low osmotic pressure (≈100 mOsmol/L), the optical quality of the shell part of the double-emulsion droplet (Figure 5b_I) was noticeably worse than when an aqueous solution containing 16 wt % sucrose and 1.8 wt % PVA with a relatively high osmotic pressure of 712 mOsmol/L was used as the external phase (Figure 5b_{II}). As shown in Figure 5c, the hypertonic external phase restricts water penetration into the shell, thereby improving the optical quality. However, due to the hypotonic core, the osmotic pressure gradient causes water to exude from the core. During this process, water molecules may bind to PEGPEA, affecting the optical quality of the resin shell, so the osmotic pressure gradient should not be excessively large.[43] Besides, the osmotic pressure gradient may cause the microcapsules to buckle (Figure S11).

Upon UV irradiation, the PEGPEA resin in the double-emulsion droplets' shell layer was polymerized, creating an elastic shell. This conferred mechanical deformability to the resulting core−shell microcapsules. During the squeeze, the shape of the microcapsules changed as well, as shown in Figure 6a. After the squeeze was released, the PEGPEA's elliptical shape reverted to a circular one. Due to the limited segmental motion, intermolecular entanglement of the polymer chains, and the time scale necessary for chain segment rearrangement, this process showed some hysteresis. Additionally, we tested the strength of a microcapsule with a diameter of 316 μm. As seen in Figures 6b and S12, the force−displacement curves show a positive linear relationship. The microcapsules were ruptured when the displacement reached 93.70 μm ($\varepsilon \approx 30\%$), and the stress was 90.77 mN. As illustrated in Figure 6c, for a minimum of 15 compression−release cycles, the microcapsules demonstrated stable responses.

To further clarify the mechanical properties of the PEGPEA resin, we conducted mechanical testing on PEGPEA resin containing 25 vol % silica: photocured dumbbell-shaped PEGPEA resin specimens were prepared via the mold-forming method using a Type 4 mold (as specified in the GB/T 528−1998 standard), with an effective test length (λ) of 10 mm. Uniaxial tensile tests were performed by using a universal material testing machine at a strain rate of 10^{-1} s^{-1}. The initial elastic modulus was determined from the slope of the tangent line in the linear elastic region of the stress−strain curve; since this material exhibits no obvious yield phenomenon, the yield stress was calculated using the specified nonproportional extension method (Rp0.2). Figure 6d presents the tensile stress−strain curve of the PEGPEA resin with 25 vol % silica. The results show that the photocured PEGPEA resin can be stretched to more than 2.5 times its original length with a tensile strength at break exceeding 0.45 MPa. In the small strain range, stress and strain exhibit an approximately linear relationship; calculations indicate that the yield stress of this resin in this stage is 0.052 MPa, and the elastic modulus is 0.11 MPa. In summary, the PEGPEA resin exhibits mechanical characteristics of low elastic modulus, low yield stress, and strain hardening after yielding under tensile conditions—reflecting a certain degree of flexibility and plastic deformation capacity, which supports the elastic deformability of the microcapsule shell.

Separately, to characterize the rheological behavior of the PNIPAM-*co*-AAC gel suspension, we performed rheological measurements using a rheometer at a frequency of 1 Hz. The storage modulus (G′) and loss modulus (G″) of the gel are shown in Figure 6e: At room temperature, G′ is greater than G″, indicating that the gel exhibits elastic-dominant viscoelastic behavior. As a classic phase-change material, PNIPAM-based gels show significant temperature-dependent rheological responses near the phase transition temperature (approximately 32 °C for the PNIPAM-*co*-AAC gel), where both G′ and G″ decrease sharply. The loss factor ($\tan\delta$ = G″/G′), a key parameter for evaluating a viscoelastic material's energy dissipation capacity and viscoelastic balance, is presented in Figure 6f: $\tan\delta$ rises from <0.3 at room temperature to a maximum of 1.12 before declining rapidly, consistent with the typical rheological characteristics of phase-change materials. Additionally, the viscosity of the gel decreases with increasing temperature, with a notably accelerated decreasing rate near the phase transition temperature (Figure 6g).

Under external pressure, the interparticle distance of the embedded silica particles dynamically adjusted with the deformation of the resin matrix. Both stretching and compression induced reversible structural color variations originating from the periodicity change in the particle array. As shown in Figure 7a, a single microcapsule was squeezed from the left and right directions toward the middle by a pair of glass plates to investigate the shell's structural color change during the deformation process. The spacing between the silica particles increased and extending outward in the section perpendicular to the compression direction, which manifested as a red shift of the structural color. Figure 7b,c illustrates the variation of reflectance wavelength for the microcapsule's shell and core with deformation degree during the squeeze-release cycle. During the squeeze process (deformation degree increasing to 30%), the reflectance wavelength of the shell showed a prominent red shift, which aligns with the structural color change induced by the increased spacing between silica particles in the shell. In contrast, the reflectance wavelength of the core remained nearly stable throughout the squeeze stage, suggesting no significant structural color variation in the core under compressive deformation (Figure 7d). As the deformation degree decreased in the release stage, the shell's reflectance wavelength decreased reversibly alongside the reduced deformation.

As schematically shown in Figure S13a, the green-shelled microcapsule was next placed on a glass slide and covered with another glass plate for pressing. The region in contact with the

https://doi.org/10.1021/acsapm.5c04701
ACS Appl. Polym. Mater. 2026, 8, 3658−3667

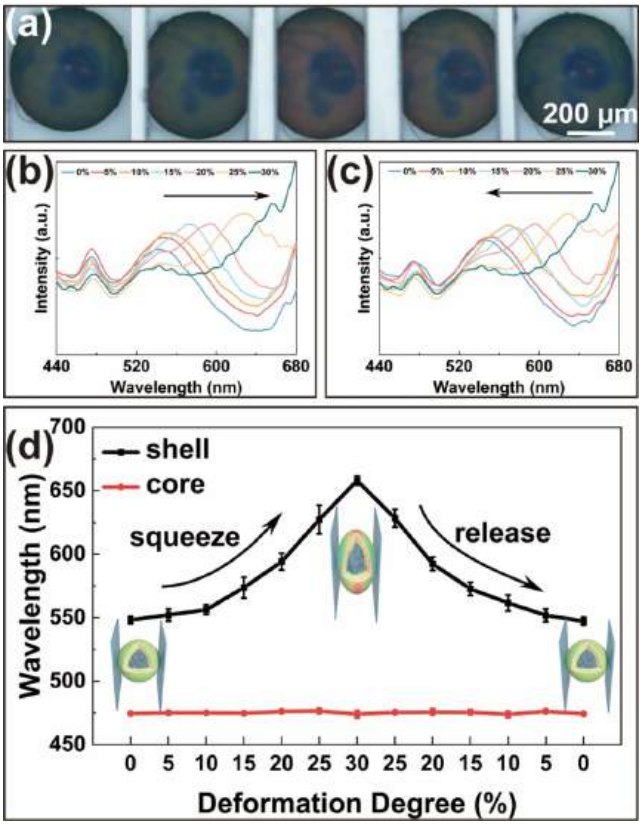

Figure 7. Optical response of the microcapsule during compression-recovery. (a) Optical microscope images of the microcapsule under varied deformation degrees (scale bar: 200 μm). (b) Reflectance spectra of microcapsules during squeezing. (c) Reflectance spectra of microcapsules during releasing. (d) Reflectance wavelength variation of the microcapsule's shell (black) and core (red) with deformation degree (from 0% to 30%, and then from 30% to 0%), error bars represent the standard deviation from five replicate measurements.

glass plate was distorted due to the pressure, which reduced the spacing of the embedded silica particles in the matrix. Upon mechanical compression, the microcapsules deformed when viewed under a microscope aligned with the extrusion direction, resulting in a noticeable blue shift of the green hue. The microcapsules took on their original shape, and the color returned to its initial state when the glass plate was lifted. The deformation-recovery process was visualized in Figure S13b and Video S2.

To demonstrate the mechanochromic advantages of the flexible PEGPEA shell, we fabricated dual-stop-band photonic microcapsules with a shell composed of ETPTA resin containing silica particles. The photocured shell is rigid, showing almost no deformation under compression, and ruptures under greater force, leading to leakage of the core photonic components into the environmental solution (Figure S14a,b). In contrast, the microcapsules proposed in this study, with shells made of photopolymerized flexible photonic resin materials, exhibit mechanochromic properties that overcome the lack of responsiveness in many similar microcapsules. Their potential applications include photonic inks and the visualization of minute stress sensing.

CONCLUSIONS

In this work, we used W/O/W double-emulsion templates to create fully deformable dual-stopband microcapsules. The microcapsules' two stopbands originated from the suspension of gel particles in the core with photonic properties and the photonic resin shell, respectively. The external phase was found to have a remarkable effect on the photonic characteristics of photonic microcapsules. Specifically, the optical quality of microcapsules was significantly better when using hypertonic solutions as the external phase compared with hypotonic ones. Following UV light curing, the PEGPEA resin substance in the shell section became highly deformable. The inner core's gel suspension increased the microcapsules' deformability due to its fluid and soft nature. This microcapsule exhibited mechanochromic characteristics since the distance between the silica particles in the shell layer changed as the flexible shell layer deformed. Potential uses in multifunctional microsensors include microcapsules with dual stopbands that produce optical signals in response to several physical inputs.

ASSOCIATED CONTENT

Supporting Information

The Supporting Information is available free of charge at https://pubs.acs.org/doi/10.1021/acsapm.5c04701.

Chemical structures of functional polymers; Controllable fabrication and structural control of double-emulsion microcapsules via microfluidics; Characterization of silica particles and gel particles; PEGPEA photonic resin with different silica volume fractions; Morphology and thermosensitivity of microcapsules; Osmotic effect and buckling of microspheres; Mechanical characterization, squeezing behavior and cracking of ETPTA-shelled microcapsules (PDF)

Process of fabricating core−shell microcapsules via microfluidics (Video S1) (MP4)

Change of the structural color of the microcapsule dynamically with deformation and recovery of the shape and color to the original state (Video S2) (MP4)

AUTHOR INFORMATION

Corresponding Author

Yuandu Hu − *Department of Materials Science and Engineering, School of Physical Science and Engineering, Beijing Jiaotong University, Beijing 100044, China; Guangdong Provincial Key Laboratory of Technique and Equipment for Macromolecular Advanced Manufacturing, South China University of Technology, Guangzhou 510641, China; Key Laboratory of Advanced Materials of the Ministry of Education, Department of Chemical Engineering, Tsinghua University, Beijing 100084, China; Hubei Provincial Key Laboratory of Green Materials for Light Industry, Hubei University of Technology, Wuhan 430068, China;* orcid.org/0000-0001-5510-2950; Email: Huyd@bjtu.edu.cn

Authors

Yu Bai − *Department of Materials Science and Engineering, School of Physical Science and Engineering, Beijing Jiaotong University, Beijing 100044, China*

Yi Ding − *Department of Materials Science and Engineering, School of Physical Science and Engineering, Beijing Jiaotong University, Beijing 100044, China*

Guoquan Liao − *Department of Materials Science and Engineering, School of Physical Science and Engineering, Beijing Jiaotong University, Beijing 100044, China*

https://doi.org/10.1021/acsapm.5c04701
ACS Appl. Polym. Mater. 2026, 8, 3658−3667

Xiangchun Kong − *Department of Materials Science and Engineering, School of Physical Science and Engineering, Beijing Jiaotong University, Beijing 100044, China*
Yucheng Wang − *Department of Materials Science and Engineering, School of Physical Science and Engineering, Beijing Jiaotong University, Beijing 100044, China*
Mingshuo Dai − *Department of Physical and Environmental Sciences, University of Toronto, Toronto, Ontario M1C 1A4, Canada*

Complete contact information is available at: https://pubs.acs.org/10.1021/acsapm.5c04701

Author Contributions

Y.B.: Investigation, writing—original draft, and funding acquisition. Y.D.: Writing—original draft. G.L.: Validation. X.K.: Validation. Y.W.: Validation. M.D.: Validation. Y.H.: Conceptualization, writing—review and editing, supervision, and funding acquisition.

Notes

The authors declare no competing financial interest.

■ ACKNOWLEDGMENTS

This work was supported by the Fundamental Research Funds for the Central Universities (No. 2025JBZX005 (Y.H.)) and (No. 2025ZYCX025 (Y.B.)). Y.H. is also grateful for the open research funds support from Guangdong Provincial Key Laboratory of Technique and Equipment for Macromolecular Advanced Manufacturing (No. 20240518), the fund from Hubei Provincial Key Laboratory of Green Materials for Light Industry, Hubei University of Technology, and Fund of Key Laboratory of Advanced Materials of Ministry of Education (Tsinghua University, No. Advmat-2402).

■ REFERENCES

(1) Isapour, G.; Lattuada, M. Multiresponsive photonic microspheres formed by hierarchical assembly of colloidal nanogels for colorimetric sensors. *ACS Appl. Nano Mater.* **2021**, *4* (4), 3389−3396.
(2) Zhao, Y. J.; Xie, Z. Y.; Gu, H. C.; Jin, L.; Zhao, X. W.; Wang, B. P.; Gu, Z. Z. Multifunctional photonic crystal barcodes from microfluidics. *NPG Asia Mater.* **2012**, *4*, No. e25.
(3) He, Q.; Ku, K. H.; Vijayamohanan, H.; Kim, B. J.; Swager, T. M. Switchable full-color reflective photonic ellipsoidal particles. *J. Am. Chem. Soc.* **2020**, *142* (23), 10424−10430.
(4) Wang, J.; Liu, Y.; Bleyer, G.; Goerlitzer, E. S. A.; Englisch, S.; Przybilla, T.; Mbah, C. F.; Engel, M.; Spiecker, E.; Imaz, I.; Maspoch, D.; Vogel, N. Coloration in supraparticles assembled from polyhedral metal-organic framework particles. *Angew. Chem., Int. Ed.* **2022**, *61* (16), No. e202117455.
(5) Wang, Y. T.; Zhang, D. G.; Zhang, H.; Shang, L. R.; Zhao, Y. J. Responsive photonic alginate hydrogel particles for the quantitative detection of alkaline phosphatase. *NPG Asia Mater.* **2022**, *14* (1), No. 54.
(6) Wang, Z.; Li, R.; Zhang, Y.; Chan, C. L. C.; Haataja, J. S.; Yu, K.; Parker, R. M.; Vignolini, S. Tuning the color of photonic glass pigments by thermal annealing. *Adv. Mater.* **2023**, *35* (34), No. e2207923.
(7) Jia, Z.; Xie, R.; Hu, Y.; Ju, X.; Wang, W.; Liu, Z.; Chu, L. Thermochromic photonic crystal microspheres with uniform color display and wide coloration range. *Macromol. Rapid Commun.* **2023**, *44* (5), No. e2200800.
(8) Lin, Z.; Gong, Z.; Bower, D. Q.; Lee, D.; Deravi, L. F. Bidispersed colloidal assemblies containing xanthommatin produce angle-independent photonic structures. *Adv. Opt. Mater.* **2021**, *9* (24), No. 2100416.
(9) Shirk, K.; Steiner, C.; Kim, J. W.; Marquez, M.; Martinez, C. J. Assembly of colloidal silica crystals inside double emulsion drops. *Langmuir* **2013**, *29* (38), 11849−11857.
(10) Li, D. Y.; Wang, W.; Chu, L. Y.; Deng, N. N. Tunable structural coloration in eccentric water-in-oil-in-water droplets. *Nano Lett.* **2023**, *23* (20), 9657−9663.
(11) Wang, L.; Chen, G.; Fan, L.; Chen, H.; Zhao, Y.; Lu, L.; Shang, L. Biomimetic enzyme cascade structural color hydrogel microparticles for diabetic wound healing management. *Adv. Sci.* **2023**, *10* (14), No. e2206900.
(12) Kim, Y. G.; Park, S.; Kim, S. H. Designing photonic microparticles with droplet microfluidics. *Chem. Commun.* **2022**, *58* (74), 10303−10328.
(13) Chen, H.; Miao, S.; Zhao, Y.; Luo, Z.; Shang, L. Rotary structural color spindles from droplet confined magnetic self-assembly. *Adv. Sci.* **2023**, *10* (8), No. e2207270.
(14) Avci, C.; De Marco, M. L.; Byun, C.; Perrin, J.; Scheel, M.; Boissiere, C.; Faustini, M. Metal-organic framework photonic balls: Single object analysis for local thermal probing. *Adv. Mater.* **2021**, *33* (43), No. e2104450.
(15) Xiao, M.; Hu, Z.; Wang, Z.; Li, Y.; Tormo, A. D.; Le Thomas, N.; Wang, B.; Gianneschi, N. C.; Shawkey, M. D.; Dhinojwala, A. Bioinspired bright noniridescent photonic melanin supraballs. *Sci. Adv.* **2017**, *3* (9), No. e1701151.
(16) Areias, L. R. P.; Marcelo, G.; Farinha, J. P. S. Polymer nanoparticle-based spherical photonic pigments for dye-free non-iridescent bright coloring. *ACS Appl. Nano Mater.* **2021**, *4* (12), 13185−13195.
(17) Yeo, S. J.; Tu, F.; Kim, S. H.; Yi, G. R.; Yoo, P. J.; Lee, D. Angle- and strain-independent coloured free-standing films incorporating non-spherical colloidal photonic crystals. *Soft Matter* **2015**, *11* (8), 1582−1588.
(18) Kim, Y. G.; Park, S.; Choi, Y. H.; Han, S. H.; Kim, S. H. Elastic photonic microcapsules containing colloidal crystallites as building blocks for macroscopic photonic surfaces. *ACS Nano* **2021**, *15* (7), 12438−12448.
(19) Xu, K.; Xu, J. H.; Lu, Y. C.; Luo, G. S. A novel method of fabricating, adjusting, and optimizing polystyrene colloidal crystal nonspherical microparticles from gas-water janus droplets in a double coaxial microfluidic device. *Cryst. Growth Des.* **2014**, *14* (2), 401−405.
(20) Kanai, T.; Lee, D.; Shum, H. C.; Shah, R. K.; Weitz, D. A. Gel-immobilized colloidal crystal shell with enhanced thermal sensitivity at photonic wavelengths. *Adv. Mater.* **2010**, *22* (44), 4998−5002.
(21) Xiao, M. Q.; Liu, J. J.; Chen, Z. J.; Liu, W. X.; Zhang, C. C.; Yu, Y. Y.; Li, C. R.; He, L. Magnetic assembly and manipulation of janus photonic crystal supraparticles from a colloidal mixture of spheres and ellipsoids. *J. Mater. Chem. C* **2021**, *9* (35), 11788−11793.
(22) Park, S.; Lee, S. S.; Kim, S. H. Photonic multishells composed of cholesteric liquid crystals designed by controlled phase separation in emulsion drops. *Adv. Mater.* **2020**, *32* (30), No. e2002166.
(23) Bai, Y.; Du, X.; Cai, Z.; Hu, Y. Advances in the construction of photonic structures with dual stopbands and beyond. *J. Mater. Chem. C* **2024**, *12* (29), 10806−10824.
(24) Kim, S. H.; Jeon, S. J.; Yi, G. R.; Heo, C. J.; Choi, J. H.; Yang, S. M. Optofluidic assembly of colloidal photonic crystals with controlled sizes, shapes, and structures. *Adv. Mater.* **2008**, *20* (9), 1649−1655.
(25) Kim, S. H.; Jeon, S. J.; Jeong, W. C.; Park, H. S.; Yang, S. M. Optofluidic synthesis of electroresponsive photonic janus balls with isotropic structural colors. *Adv. Mater.* **2008**, *20* (21), 4129−4134.
(26) Zhao, Y.; Gu, H.; Xie, Z.; Shum, H. C.; Wang, B.; Gu, Z. Bioinspired multifunctional janus particles for droplet manipulation. *J. Am. Chem. Soc.* **2013**, *135* (1), 54−57.
(27) Liu, M.; Fu, J.; Yang, S.; Wang, Y.; Jin, L.; Nah, S. H.; Gao, Y.; Ning, Y.; Murray, C. B.; Yang, S. Janus microdroplets with tunable self-recoverable and switchable reflective structural colors. *Adv. Mater.* **2023**, *35* (5), No. e2207985.
(28) Guo, Q.; Li, Y.; Liu, Q.; Li, Y.; Song, D. P. Janus photonic microspheres with bridged lamellar structures via droplet-confined

block copolymer co-assembly. *Angew. Chem., Int. Ed.* **2022**, *61* (5), No. e202113759.
(29) Yu, Z.; Wang, C. F.; Ling, L.; Chen, L.; Chen, S. Triphase microfluidic-directed self-assembly: Anisotropic colloidal photonic crystal supraparticles and multicolor patterns made easy. *Angew. Chem., Int. Ed.* **2012**, *51* (10), 2375−2378.
(30) Kim, J. B.; Kim, J. W.; Kim, M.; Kim, S. H. Dual-colored janus microspheres with photonic and plasmonic faces. *Small* **2022**, *18* (21), No. e2201437.
(31) Wang, J.; Le-The, H.; Shui, L.; Bomer, J. G.; Jin, M.; Zhou, G.; Mulvaney, P.; Pinkse, P. W. H.; van den Berg, A.; Segerink, L. I.; Eijkel, J. C. T. Multilevel spherical photonic crystals with controllable structures and structure-enhanced functionalities. *Adv. Opt. Mater.* **2020**, *8* (10), No. 1902164.
(32) Zhang, J.; Yang, S.; Tian, Y.; Wang, C. F.; Chen, S. Dual photonic-bandgap optical films towards the generation of photonic crystal-derived 2-dimensional chemical codes. *Chem. Commun.* **2015**, *51* (52), 10528−10531.
(33) Lee, J. H.; Choi, G. H.; Park, K. J.; Kim, D.; Park, J.; Lee, S.; Yi, H.; Yoo, P. J. Dual-colour generation from layered colloidal photonic crystals harnessing "core hatching" in double emulsions. *J. Mater. Chem. C* **2019**, *7* (23), 6924−6931.
(34) Zhou, C.; Zhang, S.; Hui, T.; Cui, Q.; Hu, Y. Microfluidics-assisted fabrication of dual stopband photonic microcapsules and their applications for anticounterfeiting. *Polymers* **2022**, *14* (19), No. 3954.
(35) Yang, S.; Kim, Y. G.; Park, S.; Kim, S. H. Structural color mixing in microcapsules through exclusive crystallization of binary and ternary colloids. *Adv. Mater.* **2023**, *35* (38), No. e2302750.
(36) Liu, S.-S.; Wang, C.-F.; Wang, X.-Q.; Zhang, J.; Tian, Y.; Yin, S.-N.; Chen, S. Tunable janus colloidal photonic crystal supraballs with dual photonic band gaps. *J. Mater. Chem. C* **2014**, *2* (44), 9431−9438.
(37) Ye, B.; Ding, H.; Cheng, Y.; Gu, H.; Zhao, Y.; Xie, Z.; Gu, Z. Photonic crystal microcapsules for label-free multiplex detection. *Adv. Mater.* **2014**, *26* (20), 3270−3274.
(38) Zhou, K.; Tian, T.; Wang, C.; Zhao, H.; Gao, N.; Yin, H.; Wang, P.; Ravoo, B. J.; Li, G. Multifunctional integrated compartment systems for incompatible cascade reactions based on onion-like photonic spheres. *J. Am. Chem. Soc.* **2020**, *142* (49), 20605−20615.
(39) Hu, Y.; Li, C.; Wang, J.; Jia, X.; Zhu, J.; Wang, Q.; Wang, H.; Yang, Y. Osmosis manipulable morphology and photonic property of microcapsules with colloidal nano-in-micro structure. *J. Colloid Interface Sci.* **2020**, *574*, 337−346.
(40) Kim, J. H.; Kim, J. B.; Choi, Y. H.; Park, S.; Kim, S. H. Photonic microbeads templated by oil-in-oil emulsion droplets for high saturation of structural colors. *Small* **2022**, *18* (8), No. 2105225.
(41) Kim, J. H.; Kim, J. B.; Kim, S.-H. Structural color inks containing photonic microbeads for direct writing. *ACS Appl. Mater. Interfaces* **2024**, *16* (16), 21098−21108.
(42) Choi, T. M.; Park, J.-G.; Kim, Y.-S.; Manoharan, V. N.; Kim, S.-H. Osmotic-pressure-mediated control of structural colors of photonic capsules. *Chem. Mater.* **2015**, *27* (3), 1014−1020.
(43) Kim, J. H.; Hamonangan, W. M.; Kim, S.-H. Color-tunable elastic photonic shells with high color saturation and deformability. *Adv. Opt. Mater.* **2023**, *11* (14), No. 2300085.

https://doi.org/10.1021/acsapm.5c04701
ACS Appl. Polym. Mater. 2026, 8, 3658−3667